ELSEVIER

Biochimica et Biophysica Acta 1416 (1999) 11–20

BIOCHIMICA ET BIOPHYSICA ACTA
BBA

Palmitoylation of lung surfactant protein SP-C alters surface thermodynamics, but not protein secondary structure or orientation in 1,2-dipalmitoylphosphatidylcholine Langmuir films

Carol R. Flach [a,*], Arne Gericke [b], Kevin M.W. Keough [c], Richard Mendelsohn [a]

[a] *Department of Chemistry, Rutgers University, Newark, NJ 07102, USA*
[b] *Institut für Physikalische Chemie, Martin-Luther Universität Halle, Wittenberg 06108, Halle, Germany*
[c] *Department of Biochemistry, Memorial University of Newfoundland, St. John's, Nfld., A1B 3X9, Canada*

Received 30 July 1998; received in revised form 13 October 1998; accepted 21 October 1998

Abstract

Pulmonary surfactant-specific protein, SP-C, isolated from porcine lung lavage, has been deacylated to investigate the role of the two thioester linked palmitoyl chains located near the N-terminus. Surface thermodynamic properties, secondary structure, and orientation of native and deacylated SP-C in 1,2-dipalmitoylphosphatidylcholine (DPPC) monolayers has been characterized by combined surface pressure–molecular area (π–A) isotherms and infrared reflection–absorption spectroscopy (IRRAS) measurements. The isotherms indicate that deacylation of SP-C produces more fluid monolayers at pressures less than 30 mN m^{-1}. The helical secondary structure and tilt angle (70–80° relative to the surface normal) of SP-C remained essentially unchanged upon deacylation in DPPC monolayers at a surface pressure $\sim$30 mN m^{-1}. The results are consistent with a model that acylation of SP-C may influence the rapid protein-aided spreading of a surface-associated surfactant reservoir, but not the structure of DPPC or SP-C in the monolayer at higher surface pressures.

Keywords: Lung surfactant; Infrared reflection–absorption spectroscopy; Surfactant protein C; Phospholipid; Air–water interface; Monolayer

1. Introduction

Pulmonary surfactant is a lipid–protein mixture that comprises the liquid layer lining the alveoli of the lung. The surface-active components in this mixture are thought to exist as a film in vivo which can withstand surface tension values near zero upon expiration and can facilitate the rapid spreading of surface-associated components during inhalation. The main lipid component of pulmonary surfactant, 1,2-dipalmitoylphosphatidylcholine (DPPC), is capable of lowering surface tension values to near zero upon film compression. Upon film expansion, however, DPPC does not adsorb readily and spreads too slowly to be effective in vivo [1,2]. Along with unsaturated phospholipids, two low molecular weight, hydrophobic surfactant proteins, SP-B and SP-C, have been shown to facilitate the adsorption and spreading process [3–8]. The relative amounts of the aforementioned components recovered via bronchoalveo-

* Corresponding author. Fax: +1 (973) 353-1264; E-mail: flach@andromeda.rutgers.edu

0005-2736/99/$ – see front matter
PII: S0005-2736(98)00205-3

lar lavage have been determined. DPPC constitutes approximately 30 wt% of pulmonary surfactant, unsaturated phosphatidylcholines contribute another 30%, and SP-B and SP-C together add approximately 1–2%. The majority of the remaining surfactant complex is dominated by phosphatidylglycerols, other disaturated phosphatidylcholines, and the hydrophilic surfactant protein, SP-A (for a recent review see [9]). In practice, both proteins are in use therapeutically in treating respiratory distress syndrome although, the molecular properties responsible for providing surface activity and film stability are not well defined [10].

Several structural properties of SP-C appear to be important for promoting protein–lipid interactions. SP-C is extremely hydrophobic and contains only 33–35 amino acid residues. In addition to an uninterrupted stretch of 16 aliphatic residues (Val, Ile, or Leu), the polypeptide is often post-translationally modified by the addition of two palmitoyl groups via thioester bonds to cysteine residues at positions 5 and 6 [11]. A palmitoyl group to cysteine molar ratio of approximately 1:1 has been reported for SP-C isolated from most mammalian species studied to date [9]. Other isoforms have also been identified. Canine SP-C has only one palmitoylated cysteine residue and in a recent study, 4% of the SP-C isolated from pig had an additional palmitoyl group bound to lysine-11 [12,13]. Palmitoylation via S-ester bonds, a common form of protein acylation, is thought to anchor soluble proteins to membranes. In SP-C, the dipalmitoylation imparts substantial hydrophobicity to the relatively polar N-terminus. The secondary structure of native, acylated SP-C in organic solvents has been determined by ^{1}H-NMR [14]. A very regular α-helical structure between residues 9 and 34 measuring 3.7 nm in length has been reported with a flexible, disordered N-terminal region. This length allows for hydrophobic matching between the aliphatic helical sections of SP-C and the hydrocarbon chains in a fluid DPPC bilayer.

Protein–lipid monolayers serve as good experimental models for biomembranes and are particularly well suited for investigating interactions among the surface-active components in pulmonary surfactant. Epifluorescence microscopic studies have shown that SP-C is associated with and increases the amount of fluid phase in lipid monolayers [15,16]. These studies have also indicated that there is no significant difference in domain size and shape between films containing SP-C prepared by cospreading from organic solvents compared to those resulting from the adsorption of vesicles to the air–water (a/w) interface [17,18].

Recent studies have begun to address the role of s-palmitoylation in SP-C without, however, the emergence of a consistent picture. Creuwels et al. [19] observed no significant difference in lipid adsorption to monolayers containing palmitoylated compared to non-palmitoylated recombinant SP-C, whereas a significantly reduced rate of readsorption and reduced film stability were reported for deacylated calf SP-C upon rapid cycling [20,21]. The matter is complicated by reports showing differences in helical content dependent on the method of isolation and/or of chemical depalmitoylation [9].

The relatively new technique of infrared reflection–absorption spectroscopy (IRRAS) has been used to examine the properties of pulmonary surfactant [22–25]. In the current study, this approach has been specifically applied to investigate the functional significance of the two s-palmitoyl groups in SP-C. IRRAS was first developed by Dluhy and co-workers to investigate the structural properties of insoluble monolayers at the a/w interface in situ, without the artifacts that may be introduced by Langmuir–Blodgett film transfer [26]. In addition to the structural information inherent in the IR frequencies, improvements in both theory and experiment have made the quantitative determination of the orientation of specific functional groups possible [27]. This orientational analysis was most recently applied to monolayers of DPPC and SP-C and the results provided an initial molecular-level understanding of the means by which SP-C facilitates spreading phospholipids at the a/w interface [23]. Results indicated that the helical portion of SP-C has a tilt angle of $\sim 70°$ with respect to the surface normal in DPPC monolayers at surface pressure of about 30 mN m^{-1}. The helix tilt angle for SP-C in oriented bilayers is reported as $\sim 25°$ or nearly parallel to the lipid acyl chains of DPPC [28]. The large increase in tilt when comparing bilayer to monolayer systems can be explained by hydrophobic matching between the length of the lipid acyl chains and helix. The current study further investigates the structure–function relation-

ships that exist for SP-C in lipid monolayers by utilizing IRRAS to provide information about the secondary structure and orientation of deacylated SP-C in DPPC monolayers.

2. Materials and methods

2.1. Materials

L-α-DPPC and *sn*-1 chain perdeuterated DPPC (*sn*-1 DPPC-d_{31}) were purchased from Avanti Polar Lipids (Alabaster, AL). Isotopically labeled *sn*-2 $^{13}C=O$-DPPC was generously provided by Dr. Ruthven Lewis and Professor Ronald McElhaney (University of Alberta). Chloroform, methanol, and sodium chloride were obtained from Fisher Scientific (ACS certified, Pittsburgh, PA). HPLC grade water was used (Fisher) and deuterium oxide (D_2O) with 99.9% isotopic enrichment was purchased from Isotec (Miamisburg, OH).

2.2. Protein isolation and deacylation

The protein SP-C was prepared from extracts of porcine lung lavage by the method of Bligh and Dyer [29] as described previously [30]. The purified SP-C was subjected to alkaline deacylation using a method developed by Dr. Jesus Pérez-Gil ([31] and Pérez-Gil, J., personal communication). SP-C in chloroform/methanol 1:1 (v/v) was adjusted to pH 10.5 using 0.2 M sodium carbonate. The sample was incubated for 1 h at 40°C. The materials were subjected to chromatography on Sephadex LH-60 to separate monomeric SP-C. The absence of palmitates was confirmed by electrospray mass spectrometry performed at the Department of Chemistry, University of Waterloo.

2.3. Preparation of samples and subphase for monolayer experiments

DPPC, *sn*-1 DPPC-d_{31} and *sn*-2 $^{13}C=O$-DPPC were dissolved in chloroform ($\sim$2 mg ml^{-1}) for measurements made on pure lipid monolayers. Solutions of lipid and protein (20:1 mol ratio) were prepared by mixing the appropriate amounts of chloroform/methanol (2:1, v/v) solutions of *sn*-1 DPPC-d_{31} or *sn*-2 $^{13}C=O$-DPPC ($\sim$2 mg ml^{-1}) with SP-C or deacylated SP-C (0.2–1 mg ml^{-1}). A subphase of HPLC grade H_2O was used for the IRRAS measurements on pure DPPC monolayers, whereas 0.15 M NaCl in H_2O or D_2O was used for all other experiments (pH or pD 6.0). It has been shown that the acyl chain methylene stretching bands for DPPC are not effected by the presence of salt in the subphase [32]. It was necessary to use a D_2O subphase for IRRAS measurements to avoid interference from the H_2O bending mode at $\sim$1640 cm^{-1} and to lessen the effects of the rotational–vibrational modes of H_2O vapor in the same spectral region.

2.4. Surface pressure–molecular area isotherms

A Nima Technology (Coventry, UK) model 611 Teflon trough (maximum surface area of 640 cm^2) and model PS4 surface pressure sensor using a paper Wilhelmy plate were used to acquire π–*A* isotherms. Typically, 15–30 μl of solution was spread dropwise on the surface and 30 min were allowed for solvent evaporation. All experiments were conducted at 20.5 ± 0.5°C and compression was run at 0.05 nm^2 molecule^{-1} min^{-1} for comparison of pure DPPC and *sn*-2 $^{13}C=O$-DPPC and at 0.25 nm^2 molecule^{-1} min^{-1} for comparison of pure lipid with binary mixtures of lipid with acylated and deacylated SP-C.

2.5. IRRAS measurements

A homemade Langmuir trough with a Nima model PS4 surface pressure sensor were used for the IRRAS experiments. Details of the instrument design have been described elsewhere [27]. The temperature of the subphase was 20.0 ± 0.5°C. Typically, 5–10 μl of solution were spread on a surface area of $\sim$83 cm^2. Initial surface pressure values (at maximum surface area) were 2–3 mN m^{-1} for the pure DPPC monolayers and 5–12 mN m^{-1} for the mixed lipid–protein films. Using an intermittent compression technique on our current trough design dictates these initial pressure values in order to reach a final surface pressure of $\sim$30 mN m^{-1}. After an initial relaxation period of 45 min, the film was intermittently compressed over a 3–4-h period to reach the desired surface pressure. At this final pressure, the film was allowed to relax for at least an hour prior to IR

data collection. A Bio-Rad FTS 40 A spectrometer equipped with an MCT detector (Cambridge, MA) was used. Typically, 2048 scans were acquired for s-polarization and 4096 scans for p-polarization. Interferograms were collected at 4 cm^{-1} resolution, apodized with a triangular function, and Fourier-transformed with one level of zero-filling to yield spectra encoded at 2 cm^{-1} intervals. Experiments were repeated at least five times for each angle of incidence.

2.6. Analysis of IRRAS data

Spectra were baseline corrected before peak positions and intensities were determined. IR peak positions were determined with a center of gravity algorithm using software provided by the National Research Council of Canada. All other data manipulations were performed using Grams/32 (Galactic Instruments, Salem, NH). Occasionally, residual water vapor bands were subtracted using an appropriate reference spectrum. Spectra were smoothed using a second-order, seven-point Savitsky–Golay routine before the determination of peak position and carbonyl and amide I band intensities. Peak heights rather than integrated intensities were used to minimize interference from partially overlapped spectral features. IRRAS spectra are presented as reflectance–absorbance (RA) vs. wavenumber (cm^{-1}). RA is defined as $-\log (R/R^F)$, where R is the reflectivity of the film covered surface, while R^F is the reflectivity of the film-free surface.

2.7. Determination of molecular functional group orientation

The mathematical formalism used for the simulation has been detailed elsewhere [23,27]. Briefly, the following parameters are required for the calculations. The optical set-up is characterized by the angle of incidence of the incoming beam with respect to the surface normal, ϕ_1, and the overall degree of polarization, Γ. Optical features of the subphase include the real and imaginary parts of the H_2O and D_2O refractive index, n_2 and k_2, which have been interpolated to a 1 cm^{-1} stepwidth [33]. The real part of the refractive index for the film has been obtained from IR ellipsometric measurements. The directional extinction coefficients for the monolayer, $k_x = k_y$ and k_z, are obtained using Fraser and MacRae's formalism [34] and are generated for a given tilt angle relative to the surface normal, θ, dipole moment direction relative to the local molecular axis, α, and the film extinction coefficient, k_{max}, for the particular vibration. The magnitude of k_{max} depends on the strength of the oscillation and the density of the film-forming molecules at the a/w interface which varies throughout the compression of the monolayer. Other film parameters include: the vacuum wavelength of the IR radiation at the band maximum, the full-width of the band at half-height, and the monolayer thickness, d, which can be obtained by taking into account the tilt angle for a molecule of known length, L. The angle between the dipole moment and the local molecular axis is known, leaving the tilt angle and k_{max} as unknowns. The tilt angle and k_{max} were determined by comparing measured and calculated RA values at the different angles of incidence for the two polarizations. The whole band contour was simulated and, as with the experimental bands, baseline corrected and offset to zero prior to intensity measurements.

3. Results

Surface pressure–molecular area (π–A) isotherms

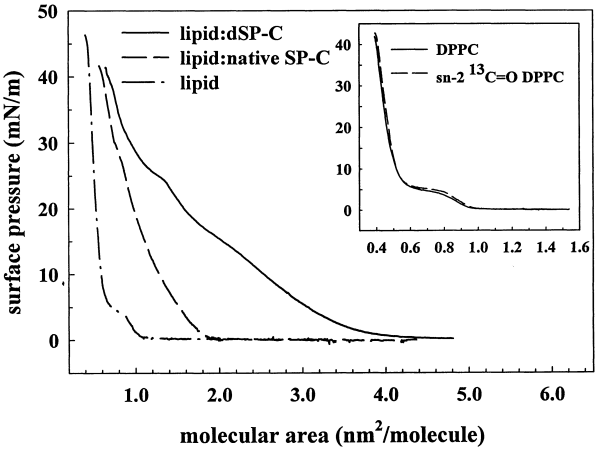

Fig. 1. Surface pressure–molecular area isotherms for lipid and lipid:protein monolayers. A subphase of 0.15 M NaCl at 20.5 ± 0.5°C was used and molecular areas are reported in terms of amount of lipid spread. The lipid referred to in the main part of the figure is *sn*-2 $^{13}C=O$-DPPC and barrier speed is 0.25 nm^2 $molecule^{-1}$ min^{-1}, whereas in the inset, barrier speed is 0.05 nm^2 $molecule^{-1}$ min^{-1}.

are displayed in Fig. 1 for pure *sn*-2 $^{13}C=O$-DPPC and binary, cospread monolayers containing the same lipid with native acylated SP-C and deacylated SP-C (dSP-C) at a lipid-to-protein mole ratio of 20:1. Molecular area is reported along the abscissa in terms of the amount of lipid spread, thereby facilitating direct comparisons between the isotherms. The inset in Fig. 1 shows that isotopic labeling of the *sn*-2 carbonyl carbon in DPPC does not significantly affect its π–*A* isotherm. The results are in good accord with those previously reported for DPPC under similar conditions [35,36]. At the lipid-to-protein ratios studied, the liquid condensed/liquid expanded (LC/LE) two-phase region at $\pi \approx 5$ mN m^{-1} for DPPC is abolished in the protein containing films. Isotherms for these two films have a slight decrease in slope at a pressure of 25–28 mN m^{-1} (Fig. 1). Possible causes of this kink include a phase change in lipid from LE to LC, a conformational or alignment change in protein, or partial loss of one or both film components to the subphase. The majority of the increase in molecular area observed at all pressures for the film containing native acylated SP-C compared to the pure lipid is most likely due to the area occupied by protein with a small portion of this area increase arising from non-ideal mixing between film components. Moderately expanded isotherms resulting from non-ideal mixing between film components have been reported previously for DPPC:acylated SP-C monolayers [6,15,37,38]. In contrast, at pressures less than 25 mN m^{-1}, a much larger increase in molecular area is observed for the film with deacylated SP-C indicating that a more liquid or expanded film exists. The diminishing difference in area between the two protein-containing films at $\pi \geq 30$ mN m^{-1} is notable and may be due to ordering or alignment in the deacylated SP-C film constituents. Overall, the π–*A* isotherms indicate that the two proteins produce films that respond differently to compression at π values below $\sim$30 mN m^{-1}. At that point, both films behave similarly and a more condensed film exists. Several IRRAS spectral parameters also suggest similarities in the two protein-containing films at high pressures ($\pi \geq 30$ mN m^{-1}).

IRRAS spectra acquired with s- and p-polarized radiation at several angles of incidence for *sn*-2 $^{13}C=O$-DPPC:dSP-C monolayers covering the 1800–1600 cm^{-1} region are displayed in Fig. 2. The unlabeled *sn*-1 carbonyl vibrational mode for DPPC is observed at $\sim$1737 cm^{-1}, whereas the *sn*-2 $^{13}C=O$ is observed at $\sim$1690 cm^{-1}. The isotopic shift of $\sim$45 cm^{-1} is anticipated due to the change in the reduced mass of the carbonyl group [39]. The protein amide I′ mode (primarily due to peptide bond C=O stretch) is observed at $\sim$1648 cm^{-1}. This band position along with the absence of amide II intensity ($\sim$1550 cm^{-1}, not shown), is indicative of a predominantly hydrogen–deuterium exchanged α-helical structure for deacylated SP-C [40]. The secondary structure of native acylated SP-C was also found to be α-helical in DPPC monolayers and bilayers [23,25,28,41]. As the angle of incident is increased from 35° to 46°, the intensities observed for the three bands increase for p-polarized radiation, whereas they remain approximately constant or slightly decrease for s-polarization. The spectra acquired using s-polarized radiation contain less noise than p-polarization due to the greater reflectivity of s-polarized light from the aqueous surface.

The IRRAS spectra shown in Fig. 2 were acquired

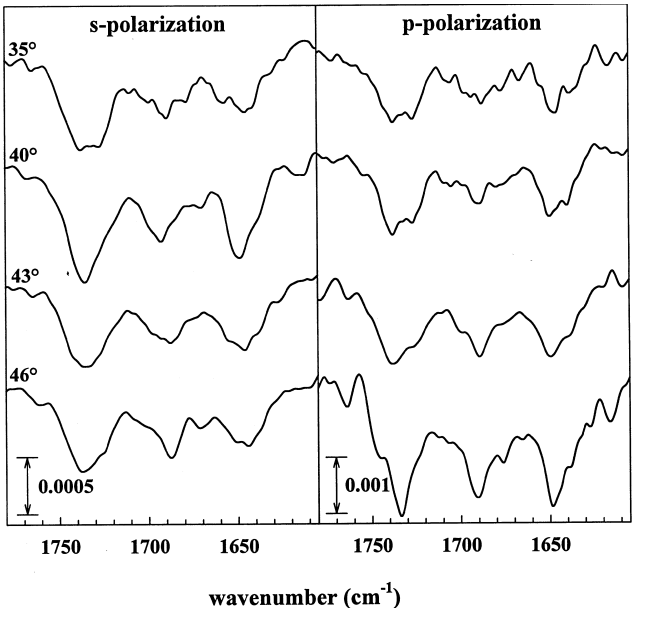

Fig. 2. IRRAS spectra of the carbonyl and amide I′ region for *sn*-2 $^{13}C=O$-DPPC:dSP-C monolayers on 0.15 M NaCl D_2O. The range of incident angles for the polarized radiation is specified on the left and surface pressure is 28 ± 2 mN m^{-1} for the intermittently compressed films at 20.0 ± 0.5°C. The bar represents the intensity in reflectance–absorbance units. Spectra are slightly smoothed (second-order, seven-point Savitzky–Golay).

over a range of incident angles so that a quantitative determination of helix orientation could be performed [23,27]. The simulations used to calculate the amide I′ band intensities and compare these with experimental values, require as input the angle between the helix axis and surface normal, and k_{max} values. The parameter k_{max} is treated as an empirical measure of the oscillator strength and the density of protein molecules sampled by the IR beam. To aid in the simulations, limiting values were required for the film parameter k_{max}. The range for this parameter was confined to ±70% of the value (k_{max} = 0.48) previously determined in simulations for native SP-C in DPPC monolayers [23]. This constraint seemed reasonable as the same conditions (lipid-to-protein ratio, same trough, initial and final pressure, and compression method) were used in the current set of experiments as in the aforementioned paper. These identical experimental conditions along with observations that helical secondary structure and average amide I′ band intensities remain approximately the same for both native and deacylated SP-C provide a rationale for limiting the range of k_{max}. Fig. 3 presents a comparison between simulated and experimental peak intensities for the amide I′ band of dSP-C in monolayers with labeled DPPC. The best fit to the experimental data was obtained with a helix tilt angle of 82° and k_{max} of 0.75. Overall, the measured intensities of the amide I′ band for the dSP-C are in the same range as those reported for the native, acylated SP-C and the derived 82° tilt is also comparable to the 70° tilt reported for the native protein.

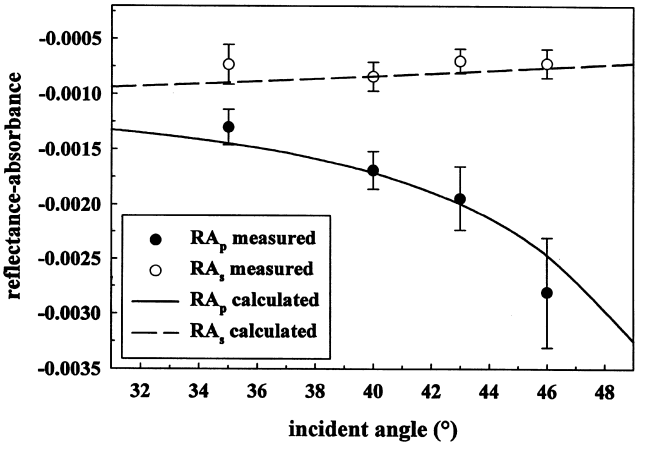

Fig. 3. Simulated and measured reflectance–absorbance intensities for the amide I′ band versus angle of incidence for *sn*-2 ^{13}C = O-DPPC:dSP-C monolayers on 0.15 M NaCl D_2O. The following parameters were used in the calculation: real part of the refractive index at the band center = 1.41, length of helix = 3.41 nm, degree of polarization = 99.5%, full-width at half-height = 18 cm^{-1}, and angle between the transition dipole and the helix axis = 28° [45]. The best fit calculated curves are shown and were obtained for k_{max} = 0.75 and helix tilt angle = 82°. The average of five measurements is shown with the spread in the data.

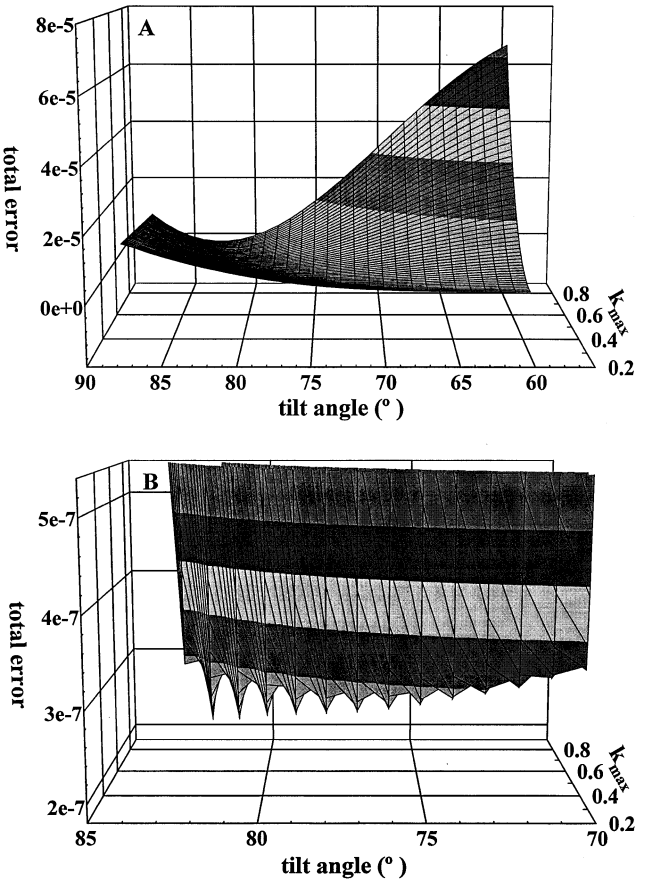

Fig. 4. 3-D plots of total error versus a limited range of tilt angles and k_{max} values for reflectance–absorbance intensities of the amide I′ band for *sn*-2 ^{13}C = O-DPPC:dSP-C monolayers. Total error represents the sum of the squares of the difference between the measured and calculated values for both polarizations at each angle of incidence. (A) displays a larger range of total error and tilt angles and in (B) the range of these values is limited to allow visualization of minimum total error. The same parameters were used as specified in Fig. 3.

To gain a better understanding of the accuracy of the simulated tilt angle, the differences between measured and calculated reflectance–absorbance intensities were squared and summed for both polar-

izations at each incident angle (total error) and are displayed in Fig. 4. The range of helix tilt angles used in the simulations for Fig. 4 was 60–88° in 1° increments and the range for k_{max} was 0.14 to 0.82 in increments of 0.01. Simulations performed over the tilt angle range of 0 to 59° resulted in larger total error values than those shown in Fig. 4A. The broad contour in Fig. 4A covers a large range of total error values and in Fig. 4B this range is narrowed to enhance the visualization of best fit tilt angles and k_{max} values. As in Fig. 3, the best fit was obtained for a helix tilt angle of 82° and k_{max} of 0.75, however, it is clear from the plot (Fig. 4B) that a range of both tilt angles and k_{max} values provides nearly indistinguishable total error values. Tilt angles from 75 to 82° and k_{max} values from 0.45 to 0.76 are found to be within 25% of the minimum total error and therefore represent a range of reasonable values. The error plots in Fig. 4B do not show monotonic behavior because calculations are performed at discrete intervals.

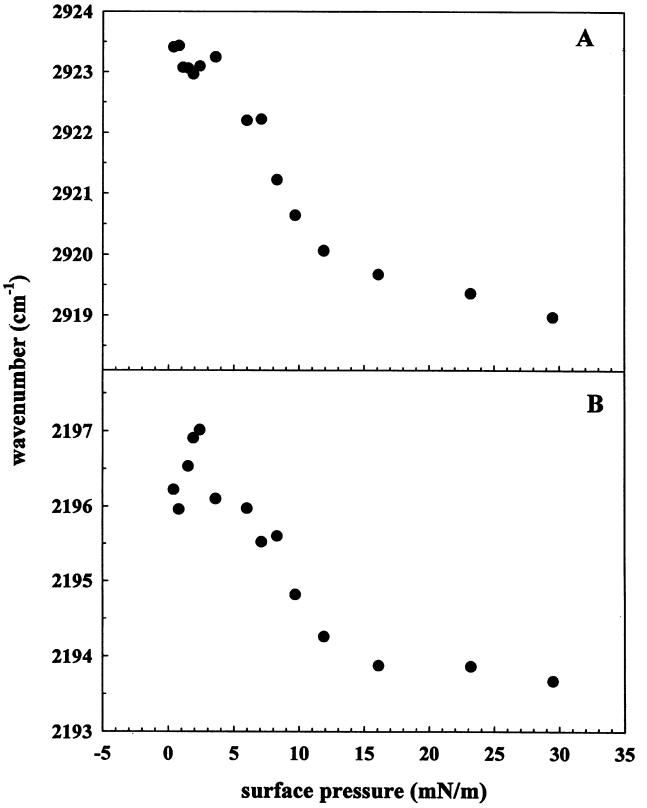

Fig. 5. Frequency of ν_aCH_2 (A) and ν_aCD_2 (B) vibrational modes versus surface pressure for an intermittently compressed *sn*-1 DPPC-d_{31} monolayer. The angle of incidence was 35° and a H_2O subphase at 20.0°C was used.

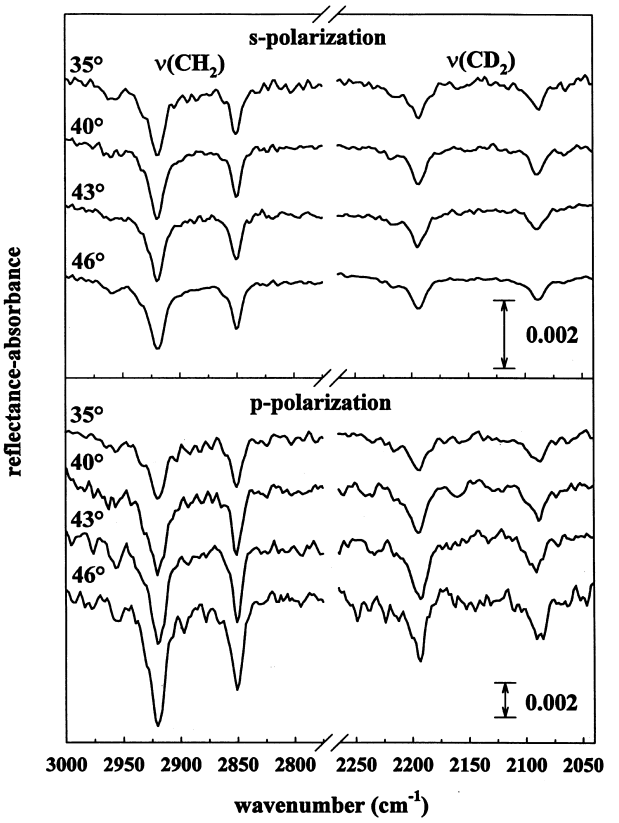

Fig. 6. IRRAS spectra of the CH_2 and CD_2 stretching region for *sn*-1 DPPC-d_{31} monolayer on H_2O subphase. The range of incident angles for the polarized radiation is specified on the left and surface pressure is 28 ± 2 mN m^{-1} for the intermittently compressed films at 20.0 ± 0.5°C. The bar represents the intensity in reflectance–absorbance units. Spectra have not been smoothed.

Fig. 5A,B displays the surface pressure induced frequency shifts for a *sn*-1 DPPC-d_{31} monolayer in the ν_aCH_2 and ν_aCD_2 vibrational modes, respectively. Pressure-induced conformational ordering of the acyl chains is observed as a frequency decrease from $\sim$2923 to $\sim$2919 cm^{-1} for the ν_aCH_2 of the *sn*-2 chain and from $\sim$2197 to $\sim$2194 cm^{-1} for the ν_aCD_2 of the *sn*-1 chain. The pressure range encompassing the ordering of both acyl chains (5–10 mN m^{-1}) is approximately the same as the range for the LE to LC plateau shown in Fig. 1 (inset) although, two different isotopically labeled DPPC films, troughs, and compression techniques were applied.

Fig. 6 displays IRRAS spectra of pure *sn*-1 DPPC-d_{31} monolayers covering CH_2 (3000–2775 cm^{-1}) and CD_2 (2250–2050 cm^{-1}) stretching regions over a range of incident angles for s- and p-polarized radi-

ation. Spectra were acquired at surface pressure of 28 ± 2 mN m^{-1} where the lipid exists in a condensed state. The average frequencies for the $\nu_a CH_2$ and $\nu_a CD_2$ vibrational modes, 2919.5 and 2193.9 cm^{-1}, respectively, indicate substantial conformational order for both acyl chains. Similar frequencies (± 0.2 cm^{-1}) and hence, similar conformational order is observed for DPPC monolayers with either native acylated or deacylated SP-C under the same experimental conditions. Attempts to quantitatively determine the tilt angles of *sn*-1 and *sn*-2 acyl chains proved difficult due to the following. First, the signal-to-noise ratio for the CH_2 stretching vibration is reduced by a factor of two compared to our previous calculation for the average tilt angle of the two chains for the unlabeled lipid [23], thereby lowering the precision of the intensities measured. Second, the extinction coefficient for the CD_2 stretching modes is less than that for corresponding CH_2 stretches, causing a further decrease in the signal-to noise-ratio for the CD_2 modes. Lastly, the nature of the calculated reflectance–absorbance properties for vibrations where the angle between the transition dipole moment change and the molecular axis is 90° (the case for CH_2 and CD_2 stretching modes) is not very sensitive to changes in axis tilt angles in the 0–25° range. Similar considerations apply to the lipid carbonyl stretching vibration for *sn*-2 $^{13}C=O$-DPPC where attempts to quantify the tilt angle between the surface normal and normal to the C=O dipole for both the *sn*-1 and *sn*-2 acyl chains were unsuccessful. These difficulties will be overcome, when improved signal-to-noise ratios allow for precise determination of reflectance–absorbance intensities.

4. Discussion

Overall, protein acylation is thought to enhance protein–membrane interaction by increasing the hydrophobicity of a protein. However, for many proteins, the specific role of lipidation has not yet been elucidated [42]. For SP-C, acylation may, at first glance, seem to be redundant since the peptide is extremely hydrophobic to begin with. The acylation motif found in SP-C is common; a thioester covalent bond is formed between a cysteine residue and palmitic acid. Other structural properties of SP-C, however, are quite unique. Two palmitoyl chains are found in SP-C for most species. These are covalently bound to two adjacent cysteine residues located near the relatively hydrophilic amino-terminus [11]. This modification introduces substantial hydrophobicity to the N-terminus of SP-C and suggests interaction with phospholipid acyl chains. The cysteines are flanked on both sides by proline residues which constrain this part of the molecule. The presence of proline may impart a particular localized secondary structure or orientation important for its interaction with lipids.

Overall, both native and deacylated SP-C have been found to enhance lipid surface activity. The expanded nature of the π–*A* isotherms for protein containing monolayers shown in Fig. 1 are consistent with those previously reported for binary mixtures of DPPC and native SP-C or fluorescein–labeled SP-C which is partially deacylated [15,37]. In addition, Crewels et al. [19] present π–*A* isotherms for pure acylated and deacylated SP-C made by recombinant DNA procedures, where the molecular areas for films of the deacylated protein are greater than those for the acylated protein. Considering the differences among the sources and labeling of SP-C, and experimental conditions, the similarities among the sets of π–*A* curves are satisfactory.

Epifluorescence microscopic results have shown that the protein is associated with the LE phase of DPPC, and that the presence of the protein results in an increase in film fluidity and decrease in the size and total amount of LC domains [16]. It was suggested that the protein-induction of fluid lipid regions would allow for faster adsorption of pulmonary surfactant upon film expansion, assuming that a lipid-rich surface-associated reservoir exists. Qanbar et al. [21], made surface activity measurements with a captive bubble surfactometer on films of DPPC, egg phosphatidylglycerol, and calf SP-C. Substantial differences were noted in lipid respreading between the films containing acylated versus deacylated protein, with the film containing deacylated SP-C losing its surface-active properties rapidly upon repeated compressions. The authors therefore suggested that acylation may be required for the formation of a lipid-rich reservoir near the surface. Wang et al. [20] also noted decreased surface activity for lipid mixtures with deacylated SP-C.

Inconsistencies exist in measurements reporting on the secondary structure of acylated compared to deacylated SP-C. An approximate 20% reduction in α-helical content has been reported for deacylated SP-C in lipid bilayers from attenuated total reflectance (ATR) FT-IR measurements [20,41] and solution circular dichroism (CD) measurements made on lipid micelles [43]. In contrast, the amide I region shown in the IRRAS spectra in Fig. 2 are qualitatively the same as those previously reported for DPPC monolayers containing native, acylated SP-C under the same experimental conditions [23]. CD measurements performed on Langmuir–Blodgett films of pure protein are also consistent with the results reported here where no significant difference is observed in the helical content of deacylated compared to acylated SP-C [19]. Thus, there appears to be slightly different effects on SP-C secondary structure induced by deacylation in bulk compared with monolayer phases. It is difficult to ascertain whether the reported differences in secondary structure are due to lipid environment, experimental parameters or the source of the SP-C. It has also been suggested that the decrease in helical content for dSP-C may be localized in the N-terminal region near the two s-palmitoylated cysteines [9].

The difficulties involved in performing quantitative IRRAS orientation measurements on monolayers at the air–water interface in situ are evident. Until the next generation of instrumentation evolves improving signal-to-noise ratios, systems for IRRAS study must be selected carefully. Under appropriate conditions, however, the advantages offered by IRRAS studies (structural and orientation information without film transfer artifacts) are substantial.

The helix axis for both acylated and deacylated SP-C, in oriented lipid bilayers, was reported as parallel to the lipid acyl chains [28,41,44]. In lipid monolayers, the helix tilt angle of SP-C (70–80°) also appears to be independent of the presence of two acyl chains. The reported tilt angles for both monolayer and bilayer environments allow for maximum hydrophobic matching between the lipid acyl chains and the helical length of SP-C. As SP-C goes from a bilayer to a monolayer environment, the increase in helix tilt would allow an increased number of DPPC molecules access to the hydrophobic helix facilitating the spread of lipid over the surface and providing the potential for very low surface tensions to be reached upon minimum molecular areas. The lack of a significant difference in the helix tilt of native SP-C compared to deacylated SP-C and epifluorescence results suggest that the acylation may not strongly influence the packing of these model systems. However, results from more dynamic surface tension measurements indicate that acylation does appear to have an important role in the formation of a surface-associated surfactant-rich reservoir. Further IRRAS studies of acylated and deacylated SP-C utilizing vesicle adsorption of isotopically labeled lipids to unlabeled monolayers may aid in clarifying the role of the s-palmitoyl chains. Structure–function relationships of SP-C can be explored further through the use of additional physiologically relevant surfactant components. Studies at lower surface pressure values may provide additional insight into the origin of the expanded isotherms generated by DPPC:deacylated SP-C.

Acknowledgements

We are grateful to Professor Ron McElhaney and Dr. Ruthven Lewis, University of Alberta, for the isotopically labeled $^{13}C=O$-DPPC. This work was supported by the US Public Health Service (Grant GM 29864 to R.M.). A.G. was supported by a fellowship from the Deutsche Forschungsgemeinschaft.

References

[1] J. Goerke, J.A. Clements, in: P.T. Mackelm, J. Mead (Eds.), Handbook of Physiology: The Respiratory System III, American Physiology Society, Washington, DC, 1986, pp. 247–261.
[2] K.M.W. Keough, in: B. Robertson, L.M.G. Van Golde, J.J. Batenburg (Eds.), Pulmonary Surfactant: From Molecular Biology to Clinical Practice, Elsevier, Amsterdam, 1992, pp. 109–164.
[3] T. Curstedt, H. Jörnvall, B. Robertson, T. Bergman, P. Berggren, Eur. J. Biochem. 168 (1987) 255–262.
[4] S. Hawgood, Am. J. Physiol. 257 (1989) L13–L22.
[5] S.-H. Yu, F. Possmayer, Biochim. Biophys. Acta 1046 (1990) 233–241.
[6] M.A. Oosterlaken-Dijksterhuis, H.P. Haagsman, L.M.G. van Golde, R.A. Demel, Biochemistry 30 (1991) 10965–10971.

[7] M.A. Oosterlaken-Dijksterhuis, H.P. Haagsman, L.M.G. van Golde, R.A. Demel, Biochemistry 30 (1991) 8276–8281.
[8] Z.D. Wang, O. Gurel, J.E. Baatz, R.H. Notter, J. Lipid Res. 37 (1996) 1749–1760.
[9] J. Johansson, T. Curstedt, Eur. J. Biochem. 244 (1997) 675–693.
[10] S. Hawgood, F.R. Poulain, Pediatr. Pulmonol. 19 (1995) 99–104.
[11] T. Curstedt, J. Johansson, P. Persson, A. Eklund, B. Robertson, B. Löwenadler, H. Jörnvall, Proc. Natl. Acad. Sci. USA 87 (1990) 2985–2989.
[12] L. Creuwels, R.A. Demel, L.M.G. Vangolde, H.P. Haagsman, Biochim. Biophys. Acta 1254 (1995) 326–332.
[13] M. Gustafsson, T. Curstedt, H. Jornvall, J. Johansson, Biochem. J. 326 (1997) 799–806.
[14] J. Johansson, T. Szyperski, T. Curstedt, K. Wuthrich, Biochemistry 33 (1994) 6015–6023.
[15] K. Nag, J. Perez-Gil, A. Cruz, K.M.W. Keough, Biophys. J. 71 (1996) 246–256.
[16] J. Pérez-Gil, K. Nag, S. Taneva, K.M.W. Keough, Biophys. J. 63 (1992) 197–204.
[17] K. Nag, J. Pérez-Gil, A. Cruz, N.H. Rich, K.M.W. Keough, Biophys. J. 71 (1996) 1356–1363.
[18] K. Nag, J. Pérez-Gil, M.L.F. Ruano, L.A.D. Worthman, J. Stewart, C. Casals, K.M.W. Keough, Biophys. J. 74 (1998) 2983–2995.
[19] L. Creuwels, R.A. Demel, L.M.G. Vangolde, B.J. Benson, H.P. Haagsman, J. Biol. Chem. 268 (1993) 26752–26758.
[20] Z.D. Wang, O. Gurel, J.E. Baatz, R.H. Notter, J. Biol. Chem. 271 (1996) 19104–19109.
[21] R. Qanbar, S. Cheng, F. Possmayer, S. Schurch, Am. J. Phys. 15 (1996) L572–L580.
[22] R.A. Dluhy, K.E. Reilly, R.D. Hunt, M.L. Mitchell, A.J. Mautone, R. Mendelsohn, Biophys. J. 56 (1989) 1173–1181.
[23] A. Gericke, C.R. Flach, R. Mendelsohn, Biophys. J. 73 (1997) 492–499.
[24] B. Pastrana-Rios, C.R. Flach, J.W. Brauner, A.J. Mautone, R. Mendelsohn, Biochemistry 33 (1994) 5121–5127.
[25] B. Pastrana-Rios, S. Taneva, K.M.W. Keough, A.J. Mautone, R. Mendelsohn, Biophys. J. 69 (1995) 2531–2540.
[26] R.A. Dluhy, J. Phys. Chem. 90 (1986) 1373–1379.
[27] C.R. Flach, A. Gericke, R. Mendelsohn, J. Phys. Chem. 101 (1997) 58–65.
[28] B. Pastrana, A.J. Mautone, R. Mendelsohn, Biochemistry 30 (1991) 10058–10064.
[29] E.G. Bligh, W.J. Dyer, Can. J. Biochem. Physiol. 37 (1959) 911–917.
[30] S.G. Taneva, J. Stewart, L. Taylor, K.M.W. Keough, Biochim. Biophys. Acta 1370 (1998) 138–150.
[31] J. Pèrez-Gil, J.L. Lopezlacomba, A. Cruz, A. Beldarrain, C. Casals, Biochem. Soc. Trans. 22 (1994) S372.
[32] C.R. Flach, J.W. Brauner, R. Mendelsohn, Biophys. J. 65 (1993) 1994–2001.
[33] J.E. Bertie, M.K. Ahmed, H.H. Eysel, J. Phys. Chem. 93 (1989) 2210–2218.
[34] R.D.B. Fraser, T.P. MacRae, Conformation in Fibrous Proteins and Related Synthetic Polypeptides, Academic Press, New York, 1973.
[35] H.M. McConnell, Annu. Rev. Phys. Chem. 42 (1991) 171–195.
[36] M.C. Phillips, D. Chapman, Biochem. Biophys. Acta 163 (1968) 301–313.
[37] S. Taneva, K.M.W. Keough, Biophys. J. 66 (1994) 1149–1157.
[38] A. Post, A.V. Nahmen, M. Schmitt, J. Ruths, H. Riegler, M. Sieber, H.-J. Galla, Mol. Membr. Biol. 12 (1995) 93–99.
[39] A. Blume, W. Hübner, G. Messner, Biochemistry 27 (1988) 8239–8249.
[40] C.R. Flach, J.W. Brauner, J.W. Taylor, R.C. Baldwin, R. Mendelsohn, Biophys. J. 67 (1994) 402–410.
[41] G. Vandenbussche, A. Clercx, T. Curstedt, J. Johansson, H. Jörnvall, J.M. Ruysschaert, Eur. J. Biochem. 203 (1992) 201–209.
[42] R.S. Bhatnagar, J.I. Gordon, Trends Cell Biol. 7 (1997) 14–20.
[43] J. Johansson, G. Nilsson, R. Stromberg, B. Robertson, H. Jornvall, T. Curstedt, Biochem. J. 307 (1995) 535–541.
[44] A. Clercx, G. Vandenbussche, T. Curstedt, J. Johansson, H. Jornvall, J.F. Ruysschaert, Eur. J. Biochem. 229 (1995) 465–472.
[45] K.J. Rothschild, N.A. Clark, Biophys. J. 25 (1979) 473–488.